Supplement of Nat. Hazards Earth Syst. Sci., 21, 2233–2244, 2021
https://doi.org/10.5194/nhess-21-2233-2021-supplement

Natural Hazards and Earth System Sciences
Open Access
EGU

Supplement of

Spatiotemporal heterogeneity of b values revealed by a data-driven approach for the 17 June 2019 M_S 6.0 Changning earthquake sequence, Sichuan, China

Changsheng Jiang et al.

Correspondence to: Changsheng Jiang (jiangcs@cea-igp.ac.cn)

Supplement

The Influence of the Uncertainty of Focal Depth on the Distribution of *b* Values

The uncertainty of the earthquake focal depth calculated by the HypoDD method is statistically about 0.654 km in this paper, but the true uncertainty of the focal depth may exceed the theoretical uncertainty given by the relocation method. Thus, the potential influence of the uncertainty of seismic depth must be considered for the reliability of the distribution characteristics of *b* values on the depth profile.

In order to study the above problem, we conducted random disturbance tests on the locations of the earthquake sources in Figure 4c. We performed a random disturbance of ±1km on the horizontal position of the earthquakes, and used the uncertainty of ±2km, ±4km and the random distribution in the range of [-22km 0km] to disturb the original depths respectively. Considering the distribution density of seismic stations in the study area, the above-mentioned disturbance scales of 2km and 4km for the focal depth should reach or exceed the uncertainty of the true focal depth. In the process of generating the random earthquake catalog, in order to prevent the occurrence of "air-quake" with depth ≥0 km, we force the random disturbance to continue until the depth <0 m. The distribution of *b* values recalculated by using the above three new earthquake catalogues is shown in Figure S1 (a), (b) and (c), respectively.

The random test results show that the difference between the *b* values distribution and Figure 4c is not significant when the depth disturbance scale is ±2km, and the *b* values distribution can be kept similar even when the disturbance scale reaches ±4km. But when the depth is a random number in the range of [-22km 0km], the characteristic distribution of *b* values on the depth profile disappears. The above three random test results imply that the uncertainty of depth is difficult to significantly affect the characteristic distribution of *b* values in Figure 4c. According to the above three random test results, it is difficult for the uncertainty of depth to have a significant effect on the characteristic distribution of *b* values on the depth profile in Figure 4c.

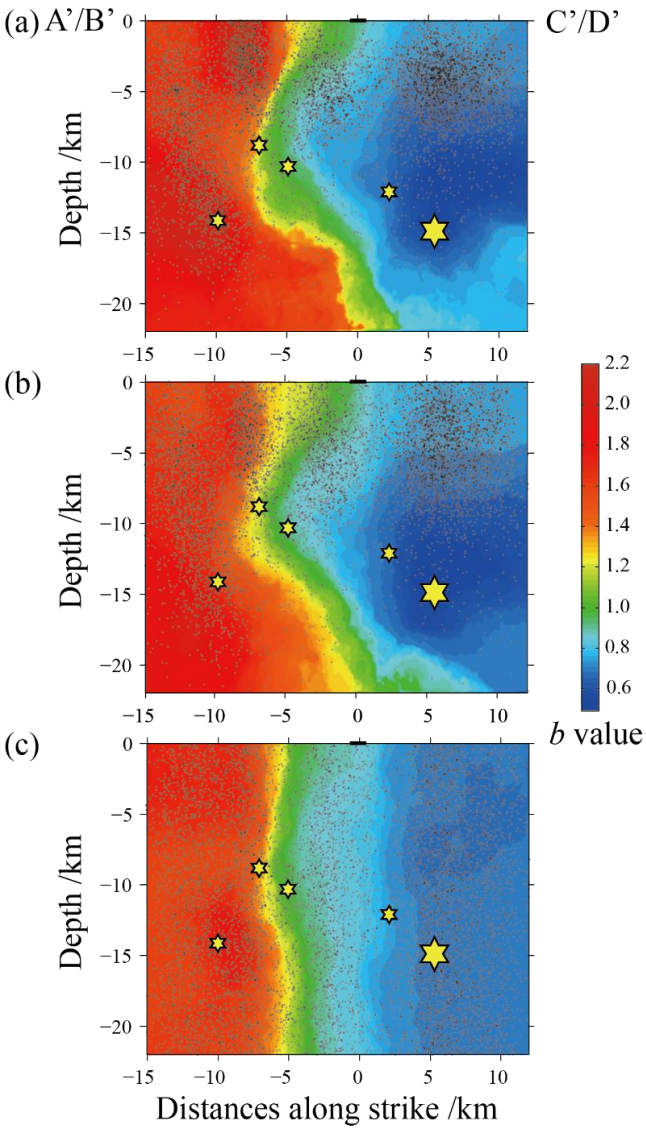

Fig. S1 The spatial distribution of the ensemble median *b* values on the depth profile obtained after random perturbation experiments on the focal depth in Figure 4c. (a) Distribution of ensemble median *b* values calculated from the earthquake catalog obtained by ±1km disturbance in horizontal position and ±2km disturbance in depth; (b) Distribution of ensemble median *b* values calculated from the earthquake catalog obtained by ±1km disturbance in horizontal position and ±4km disturbance in depth; (c) Distribution of ensemble median *b* values calculated from the earthquake catalog obtained by ±1km disturbance in horizontal position and random distribution in depth. The black dots mark the seismic events whose locations are randomly disturbed and used for *b* values calculation. The hexagonal star marks the locations of the mainshock and four aftershocks with magnitude no less than 5.0 that have undergone random disturbances.

The Distribution of Ensemble *b* Values and Ensemble MAD *b* Values Calculated Using the Mainshock and Aftershocks

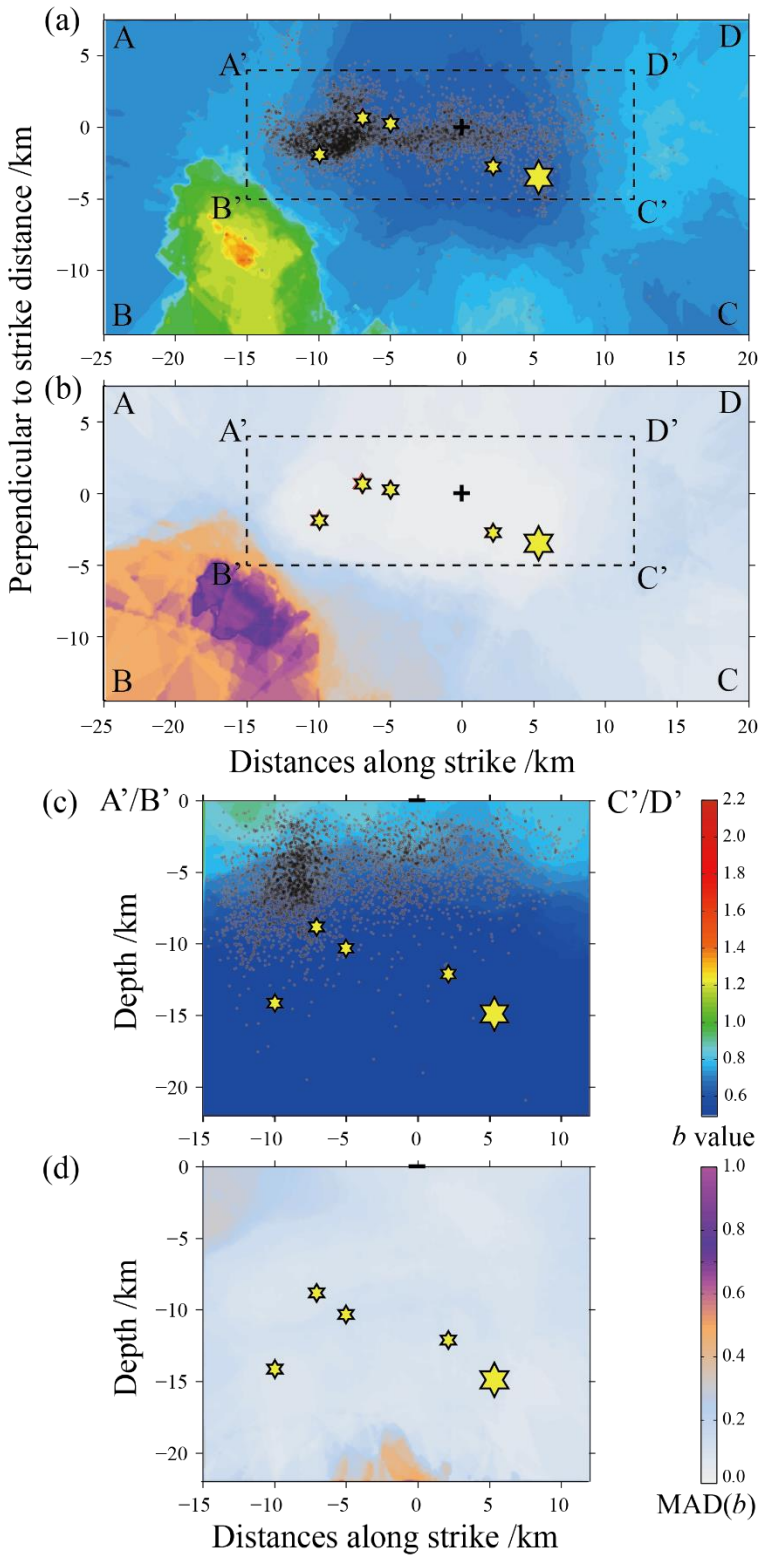

Fig. S2 The spatial distribution of the ensemble median *b* values and MAD *b* values of the best-100 solutions after the Changning M_S 6.0 earthquake. (a) The ensemble median *b* values is distributed on the horizontal plane after the rotation; (b) The ensemble MAD *b* values is distributed on the horizontal plane after the rotation; (c) Distribution of the ensemble median

***b* values in the rectangular frame A'B'C'D' on the depth profile; (d) Distribution of ensemble MAD *b* values in the rectangular frame A'B'C'D' on the depth profile. The black dots mark the seismic events used in the calculation.**

Temporal Variation of *b* Values before the Mainshock

In order to verify the reliability of the spatiotemporal evolution of *b* values before the Changning earthquake in Figure 6b, we reduce the dimension and only investigate the temporal variation of *b* values. According to the temporal and spatial evolution characteristics of *b* values, we divide the region A'B'C'D' into three sections, Section 1 with lower *b* values uniformly and stably distributed in time and space and containing the nucleation point of mainshock, Section 2 with higher *b* values extending to the nucleation point, and section 3 with higher *b* values always distributed. We used a fixed window of 300 seismic events and a window of gradual cumulative increase with 300 seismic events. In both methods, the earthquakes are selected and calculated retrospectively from the failure time of the mainshock to the past, and the calculation is stopped when there are less than 300 events in the current window/step. The reason why we use 300 earthquake windows/steps subjectively is to ensure the statistical reliability when fitting the OK1993 model, and to obtain more results of temporal variations of *b* values at the same time.

The results (Figure S3) show that the temporal variations of the *b* values of segment 1 is very stable and maintains a lower value (about 0.75), the *b* values of segment 2 continuously increases from 0.8 to about 1.2, and the *b* values of segment 3 is always greater than 1.0 and it climbed rapidly about one year before the mainshock. The temporal variations of *b* values of three segments are highly consistent with the spatiotemporal migration pattern in Figure 6b, which further verifies the reliability of Figure 6b. it is also confirmed that the area where the nucleation point is located has stable lower *b* values on the long-term scale close to 10 years before the mainshock.

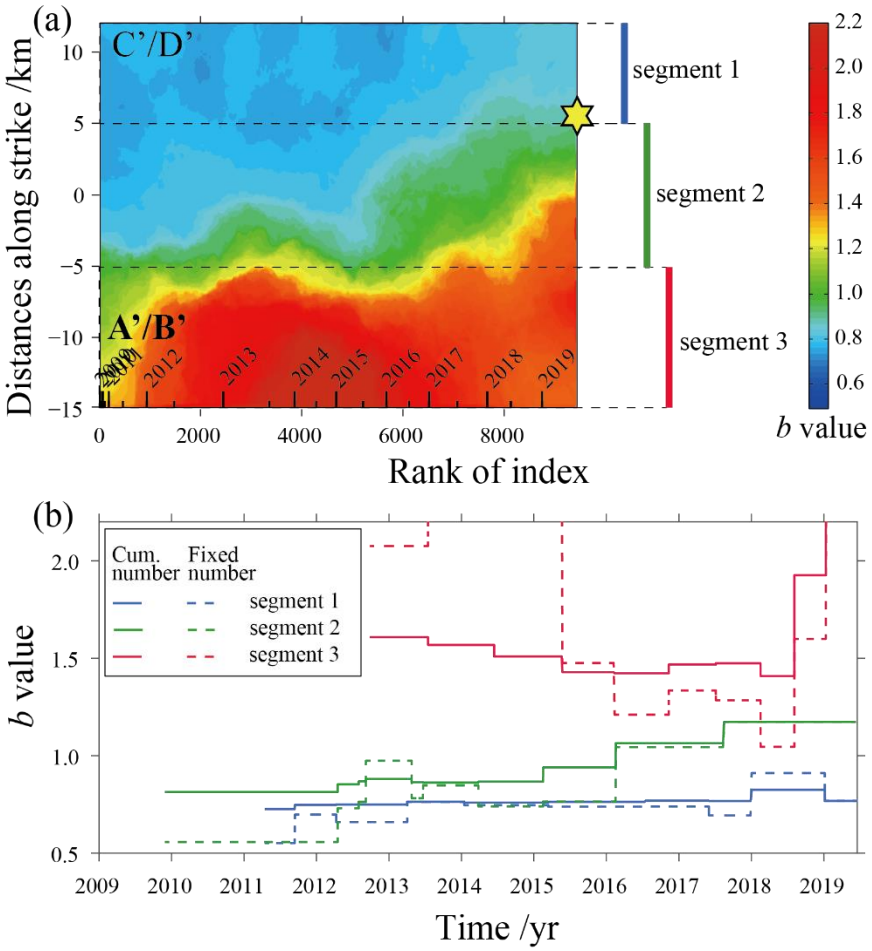

Fig. S3 The temporal variations of the *b* values before the Changning earthquake. (a) The temporal and spatial distribution of *b* values (Figure 6b) before the Changning earthquake and the division of spatial segments (Segment 1, 2 and 3) for the study of temporal variations of the *b* values. (b) The temporal variations of the *b* values in three segments before the Changning earthquake. The solid lines and the dashed lines respectively represent the *b* value results obtained by using a fixed window of 300 seismic events and a window of gradual cumulative increase with 300 seismic events, and different colors indicate the results on different segments.

Minimum Completeness Magnitude and its Influence on the Calculation of *b* Values

The analysis of the minimum completeness magnitude M_c of the earthquake catalog is an important basis for the calculation of *b* value. In the traditional *b* value calculation based on the G-R relationship, the accurate calculation of M_c and the reasonable selection of the cut-off magnitude will affect the results of *b* value (Harte, 2016). Since the OK1993 model in this paper is a model that uses a continuous function to describe the magnitude-frequency distribution, all events including incompletely recorded events are used for model fitting, so there is no need to select the cut-off magnitude. In addition, the M_c and *b* values are obtained at the same time when fitting the OK1993 model, so the M_c will not affect the result of the *b* values, which is the inherent advantage of the OK1993 model.

According to the estimation results of Mignan and Woessner (2012) and Iwata (2013), the minimum magnitude of completeness M_c related to OK1993 model can be approximately expressed by using $\mu+2\sigma$ or $\mu+3\sigma$, which

represents the complete record of magnitude at the 95% or 99.9% confidence level. In this paper, we chose $\mu+2\sigma$ as the M_c, and gave the distribution of $M_c(\mu+2\sigma)$ during the calculation of b values on the horizontal plane, depth profile, and 2-D spatiotemporal dimension (Figure S3). In this paper, we chose $\mu+2\sigma$ as the M_c and mark it as $M_c(\mu+2\sigma)$. The distribution of $M_c(\mu+2\sigma)$ obtained at the same time when calculating the b values on the horizontal plane, the depth profile and the 2-D spatiotemporal dimension is shown in Figure S4. It can be seen from Figure S3 that the $M_c(\mu+2\sigma)$ in the study area ABCD is mainly distributed between 0.7 and 1.6, and the $M_c(\mu+2\sigma)$ in the East is smaller than that in the West, which is consistent with the distribution characteristics of seismic stations in Figure 1. In addition, the distribution characteristics of $M_c(\mu+2\sigma)$ are not the same as the b values, which can rule out the dependence of the b values on $M_c(\mu+2\sigma)$ to a certain extent.

In order to further verify whether the $M_c(\mu+2\sigma)$ has an impact on the calculation of the b values, we randomly deleted 13.5% of the 18371 events (the same as the number of events lost in the relocation) in space and recalculated the b values of Figure 4a and the uncertainty of Figure 5a. The Figure S5 show that the distribution of the b values and its uncertainty obtained after this loss of part of the events is still relatively close to Figure 4a and Figure 5a, which also implies that the minimum completeness magnitude will not significantly affect the results of this paper.

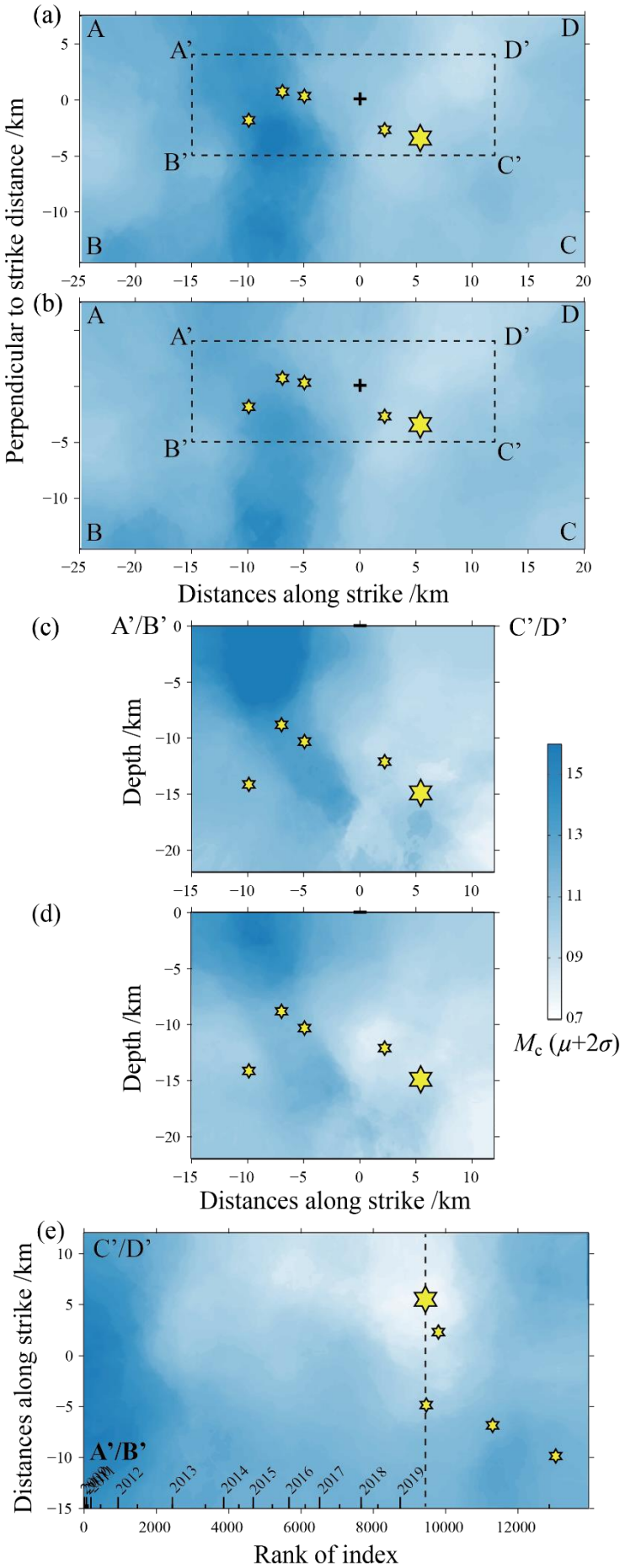
(a)
A
D
A'
D'
B'
C'
B
C
(b)
Perpendicular to strike distance /km
Distances along strike /km
(c)
A'/B'
C'/D'
Depth /km
(d)
Depth /km
Distances along strike /km
15
13
11
09
07
M_c (μ+2σ)
(e)
C'/D'
A'/B'
Distances along strike /km
2011
2012
2013
2014
2015
2016
2017
2018
2019
Rank of index

Fig. S4 Distribution of minimum magnitude of completeness $M_c(\mu+2\sigma)$. (a) Distribution of $M_c(\mu+2\sigma)$ on the horizontal plane after the rotation calculated by the events before the Changning M_S 6.0 earthquake; (b) Distribution of $M_c(\mu+2\sigma)$ on the horizontal plane after the rotation calculated by all the events including the aftershocks of the Changning M_S 6.0 earthquake; (c) Distribution of $M_c(\mu+2\sigma)$ in the rectangular frame A'B'C'D' on the depth profile calculated by the events before the Changning M_S 6.0 earthquake; (d) Distribution of $M_c(\mu+2\sigma)$ in the rectangular frame A'B'C'D' on the depth profile calculated by all events including aftershocks of the Changning M_S 6.0 earthquake. The hexagonal star marks the locations of the mainshock and four aftershocks with magnitude no less than 5.0.

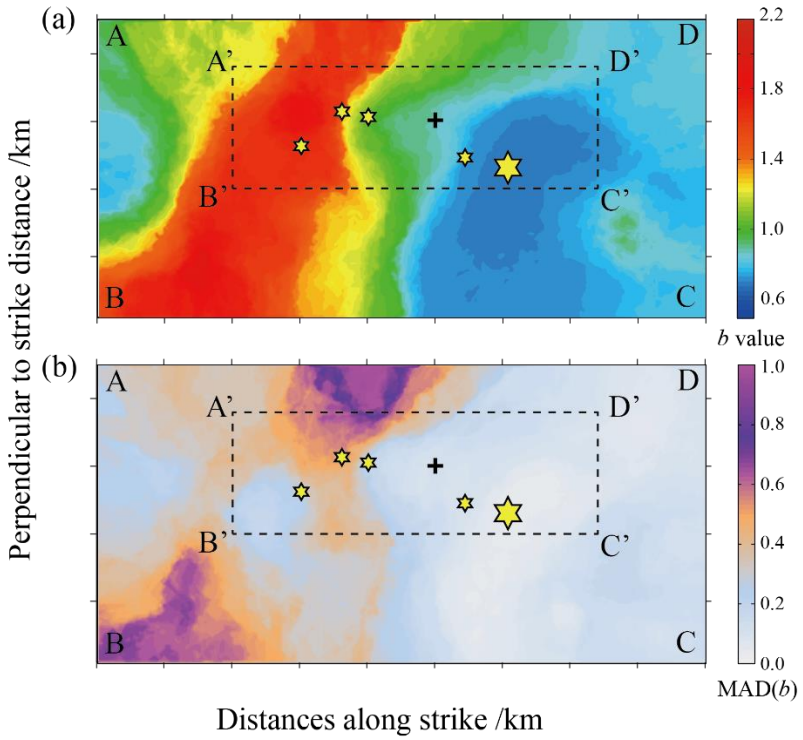

Fig. S5 Distribution of the ensemble *b* values (a) and MAD *b* values (b) of the best-100 solutions prior to the Changning M_S 6.0 earthquake, in which the events used were randomly deleted from 13.5% of the 18371 events.

References

Harte, D. S. (2016). "Model parameter estimation bias induced by earthquake magnitude cut-off". Geophysical Journal International **204**(2): 1266-1287.

Iwata, T. (2013). "Estimation of completeness magnitude considering daily variation in earthquake detection capability". Geophysical Journal International **194**: 1909-1919.

Mignan, A., Woessner, J. (2012). "Estimating the magnitude of completeness for earthquake catalogs. " CORSSA: Community Online Resource for Statistical Seismicity Analysis. doi: 10.5078/corssa-00180805.